STM JOURNALS

Journal of
Polymer & Composites

ISSN: 2321-2810 (Online)
ISSN: 2321-8525 (Print)
Volume 14, Special Issue 3, 2026
DOI (Journal): 10.37591/JoPC

https://journals.stmjournals.com/jopc

Research JoPC

Bonding Strength Characteristics of FRP Cylindrical Composites Under Hygrothermal Loading

Kunal Pradhan[1], T. Malyadri[2,*], G. Srinivasa Gupta[3]

Abstract

This study investigates the bonding strength characteristics and stress distribution patterns in fiber-reinforced polymer (FRP) cylindrical composites subjected to hygrothermal loading conditions. A four-phase cylindrical model incorporating AS-Graphite and S-Glass fibers with low modulus epoxy coating was analyzed under four distinct pressure loading conditions (25.984, 38.976, 77.953, and 155.906 MPa). Comprehensive stress analysis revealed significant variations in von-Mises stress, maximum principal stress, and minimum principal stress across fiber, coating, matrix, and composite phases. AS-Graphite composites exhibited superior stress resistance, with maximum von-Mises stress of 148.86 MPa at the highest loading, representing 50.7% lower stress magnitude compared to S-Glass composites (302.05 MPa) under identical conditions. The low modulus coating layer demonstrated critical stress mitigation functionality, reducing interfacial stress concentrations by 47-52% at fiber-coating boundaries. Stress concentration mechanisms were predominantly governed by elastic modulus mismatch and hygrothermal expansion coefficient differentials between constituent phases. Results indicate that coating layer effectiveness and fiber type selection are paramount design considerations for hygrothermal environments, with AS-Graphite systems providing enhanced structural integrity and bonding performance.

Keywords: FRP composites, hygrothermal loading, bonding strength, stress distribution, AS-Graphite fiber, S-glass fiber, interfacial mechanics

INTRODUCTION

Fiber-reinforced polymer (FRP) composites have emerged as critical structural materials in aerospace, marine, civil infrastructure, and energy sectors due to their exceptional strength-to-weight ratios, corrosion resistance, and design flexibility. However, the long-term durability and structural integrity of FRP composites are significantly compromised when exposed to hygrothermal environments, where simultaneous moisture absorption and temperature fluctuations induce complex degradation mechanisms [6, 16]. The bonding strength between constituent phasesfiber, matrix, and interfacial coating layersrepresents a critical performance parameter that governs load transfer efficiency, stress distribution patterns, and ultimate failure modes in cylindrical composite structures.

***Author for Correspondence**
T. Malyadri

[1]M. Tech Student, Department of Mechanical Engineering, VNR Vignana Jyothi Institute of Engineering and Technology, Hyderabad, Telangana, India
[2]Assistant Professor, Department of Mechanical Engineering, VNR Vignana Jyothi Institute of Engineering and Technology, Hyderabad, Telangana, India
[3]Professor, Department of Mechanical Engineering, VNR Vignana Jyothi Institute of Engineering and Technology, Hyderabad, Telangana, India

Received Date: May 12, 2026
Accepted Date: June 10, 2026
Published Date: June 20, 2026

Citation: Kunal Pradhan, T. Malyadri, G. Srinivasa Gupta. Bonding Strength Characteristics of FRP Cylindrical Composites Under Hygrothermal Loading. Journal of Polymer & Composites. 2026; 14(Special Issue 3): S950–S967p.

Recent investigations have demonstrated that hygrothermal conditioning induces multiscale degradation phenomena, including matrix plasticization, fiber-matrix debonding, interfacial weakening, and residual stress development [6. 17, 19] reported transverse tensile strength reductions of 72% and shear strength degradation of 13% in thick composites subjected to severe hygrothermal conditions. Similarly [9], documented accelerated

aging mechanisms in E-glass fiber reinforced epoxy pipes, attributing failure to progressive interfacial deterioration and stress concentration amplification. The complexity of hygrothermal effects is further compounded in cylindrical geometries, where free-edge stress fields and interlaminar stress concentrations are exacerbated by moisture-induced swelling and thermal expansion mismatches [7].

The role of interfacial coating layers in mitigating hygrothermal degradation has received increasing attention in recent literature [10–11]. demonstrated that epoxy-coated glass fiber composites exhibited enhanced flexural and interlaminar shear strength retention compared to uncoated systems under simulated hygrothermal environments. The coating layer functions as a protective barrier against moisture ingress while simultaneously accommodating elastic modulus transitions between high-stiffness fibers and compliant matrix materials. However, the stress distribution characteristics and bonding strength evolution in multi-phase cylindrical composites incorporating low modulus coatings remain inadequately characterized, particularly under progressive loading conditions.

Comparative studies of different fiber reinforcement systems have revealed substantial performance variations under hygrothermal exposure. Carbon-based fibers, including AS-Graphite variants, generally exhibit superior moisture resistance and dimensional stability compared to glass fiber systems [12, 15] Nevertheless, the specific stress distribution patterns, interfacial bonding characteristics, and failure mechanisms in AS-Graphite versus S-Glass cylindrical composites under hygrothermal loading have not been systematically quantified. Understanding these comparative performance metrics is essential for material selection and structural design optimization in hygrothermal service environments.

This investigation addresses critical knowledge gaps by providing comprehensive stress analysis of AS-Graphite and S-Glass fiber cylindrical composites with low modulus epoxy coating under four progressive hygrothermal loading conditions. The study objectives are: (1) to quantify stress distribution patterns across fiber, coating, matrix, and composite phases; (2) to evaluate comparative bonding strength characteristics between AS-Graphite and S-Glass systems; (3) to elucidate stress concentration mechanisms at interfacial boundaries; (4) to assess coating layer effectiveness in stress mitigation; and (5) to provide engineering insights for hygrothermal-resistant composite design. The findings contribute fundamental understanding of multi-phase stress evolution and interfacial mechanics in cylindrical FRP composites subjected to hygrothermal loading.

BACKGROUND AND THEORETICAL FOUNDATIONS

Hygrothermal Degradation Mechanisms in FRP Composites

Hygrothermal degradation in fiber-reinforced polymer composites represents a complex, multi-mechanism phenomenon involving coupled moisture diffusion, thermal cycling, and mechanical stress interactions. Moisture absorption in polymer matrices follows Fickian or non-Fickian diffusion kinetics, depending on temperature, relative humidity, and matrix chemistry [13]. The absorbed moisture induces matrix plasticization through hydrogen bonding disruption and free volume expansion, resulting in reduced glass transition temperature and elastic modulus degradation [2–4]. Concurrently, differential hygroscopic expansion between hydrophilic matrices and hydrophobic fibers generates internal residual stresses that compromise interfacial bonding integrity.

The fiber-matrix interface constitutes the most vulnerable region for hygrothermal attack due to inherent chemical and mechanical property discontinuities. Moisture preferentially accumulates at interfacial regions, catalyzing hydrolytic degradation of sizing agents and coupling agents that facilitate load transfer [8]. This interfacial weakening manifests as progressive debonding, reduced shear strength, and premature failure under mechanical loading. Recent multiscale modeling approaches have demonstrated that hygrothermal-induced property degradation is spatially heterogeneous, with outer layers experiencing more severe degradation than interior regions due to moisture concentration gradients [6].

Stress Distribution in Cylindrical Composite Structures

Cylindrical composite structures exhibit complex three-dimensional stress states characterized by radial, circumferential, and axial stress components. Under internal pressure loading, the stress distribution is governed by classical laminated shell theory, modified by hygrothermal effects that alter material properties and introduce additional stress components [7, 14]. The free-edge effect in cylindrical laminates generates significant interlaminar normal and shear stresses near geometric discontinuities, which are further amplified by moisture-induced swelling and thermal expansion mismatches.

Three-dimensional exact shell models incorporating hygro-elastic coupling effects developed [5], demonstrating that moisture content significantly influences stress field distributions in layered composite structures. The stress concentration at fiber-matrix interfaces is particularly pronounced in cylindrical geometries due to elastic modulus mismatches and Poisson's ratio differentials. The stress concentration factors at fiber-matrix boundaries can exceed 3.0 in underground reinforced plastic pipes, with fracture toughness being critically dependent on interfacial bonding quality [1].

Role of Coating Layers in Interfacial Mechanics

Interfacial coating layers serve multiple functions in composite systems: (1) protection against environmental degradation, (2) stress gradient accommodation between dissimilar materials, and (3) enhancement of load transfer efficiency. Low modulus coatings are particularly effective in reducing stress concentrations at fiber-matrix boundaries by providing a compliant interlayer that accommodates elastic modulus transitions (Manalo et al., 2022). The coating layer thickness, elastic properties, and adhesion characteristics critically influence overall composite performance under hygrothermal conditions.

In [18], interfacial cracking between epoxy-based composite coatings and rigid substrates under thermal loading was investigated, and the critical stress intensity factors along with the underlying crack propagation mechanisms were identified. The study revealed that coating layer compliance significantly affects interfacial stress distribution and crack initiation thresholds. Similarly, [16] adhesive parameters optimized for CFRP-Al bonded structures in hygrothermal environments, demonstrating that interfacial bonding strength is highly sensitive to moisture content and temperature variations.

Comparative Performance of Carbon and Glass Fiber Systems

Carbon-based fibers (including AS-Graphite variants) and glass fibers exhibit fundamentally different hygrothermal response characteristics due to their distinct chemical compositions, microstructures, and surface properties. The hydrophobic nature of carbon fibers results in negligible moisture absorption, while glass fibers experience strength degradation under humid conditions as a consequence of stress-corrosion mechanisms [19]. In contrast, basalt fiber composites reinforced with graphene nanoplatelets have been shown to maintain superior mechanical performance following hydrothermal aging relative to traditional glass fiber-reinforced systems [12].

Differences in the coefficients of thermal expansion (CTE) of fibers and polymer matrices lead to the development of thermal residual stresses during both manufacturing and service life. Carbon fibers generally possess negative or near-zero axial CTE values, whereas glass fibers exhibit positive CTE values that are more compatible with those of polymer matrices. These variations significantly affect stress distribution and interfacial adhesion when composites are subjected to thermal cycling [5]. Recent studies have indicated that hybrid carbon–glass fiber composites offer improved hygrothermal performance by combining the superior moisture resistance and thermal stability of carbon fibers with the economic advantages and complementary properties of glass fibers [19, 17].

MATERIALS AND METHODS

Material Systems

Two distinct fiber reinforcement systems were investigated in this study: AS-Graphite (AS4 carbon fiber) and S-Glass fibers, both embedded in epoxy resin matrix with low modulus epoxy coating interlayers. The AS-Graphite fiber system represents a high-performance carbon fiber variant characterized by high tensile strength (3.65 GPa), high elastic modulus (231 GPa), and excellent environmental resistance. The S-Glass fiber system, widely utilized in marine and chemical processing applications, exhibits moderate tensile strength (4.58 GPa), lower elastic modulus (86.9 GPa), and superior impact resistance compared to carbon fibers.

The low modulus epoxy coating layer was applied at the fiber-matrix interface to enhance bonding characteristics and mitigate stress concentrations. The coating material was selected for its compliance (elastic modulus approximately 2.5–3.5 GPa), excellent adhesion to both fiber and matrix phases, and moisture barrier properties. The epoxy resin matrix system consisted of a standard bisphenol-A based epoxy with amine hardener, exhibiting elastic modulus of approximately 3.2 GPa and glass transition temperature of 120°C in the unconditioned state.

Four-Phase Cylindrical Model Configuration

A four-phase cylindrical composite model was developed to represent the hierarchical structure of coated fiber-reinforced composites. The model geometry consisted of concentric cylindrical regions representing: (1) fiber core (inner radius 3.8 mm to outer radius 19.3 mm), (2) coating layer (19.3 mm to 20.9 mm), (3) matrix region (20.9 mm to 24.8 mm), and (4) composite outer region (24.8 mm to 34.8 mm). This configuration enabled systematic evaluation of stress distribution across distinct material phases and interfacial boundaries.

The cylindrical geometry was selected to represent typical filament-wound pressure vessel and pipe configurations commonly employed in hygrothermal service environments. The radial dimension progression allowed for detailed stress field characterization from the fiber core through successive interfacial regions to the outer composite surface. Material property assignments for each phase incorporated temperature and moisture-dependent degradation factors based on established hygrothermal aging models.

Loading Conditions and Hygrothermal Environment

Four progressive internal pressure loading conditions were applied to simulate service load ranges in hygrothermal applications: (1) 25.984 MPa (100 kN equivalent force), (2) 38.976 MPa (150 kN), (3) 77.953 MPa (300 kN), and (4) 155.906 MPa (600 kN). These loading magnitudes represent low, moderate, high, and extreme pressure scenarios encountered in marine pipelines, chemical processing equipment, and aerospace pressure vessels.

Hygrothermal conditioning was accounted for by applying material property degradation factors obtained from accelerated aging experiments and published literature. The environmental conditions were set at 70°C and 85% relative humidity to represent severe marine or tropical service environments. An epoxy matrix moisture uptake of approximately 1.5–2.0 wt.% was considered, resulting in reductions in elastic modulus of about 15–20% and a decrease in glass transition temperature of 25–30°C, in agreement with the hygrothermal degradation characteristics reported in the literature [6, 9].

Based on widely used accelerated aging techniques documented in the literature for FRP composites, the hygrothermal exposure settings of 70°C and 85% relative humidity were chosen. These circumstances mimic harsh marine and tropical environments where diffusion processes, matrix plasticization, and interfacial degradation are accelerated by high temperatures and wetness. According to earlier research, exposure at 70°C and 85% relative humidity efficiently replicates long-

term service degradation mechanisms in a shorter amount of time, which makes these settings appropriate for assessing FRP systems' resilience in harsh environmental circumstances.

Stress Analysis Methodology

Comprehensive stress analysis was conducted to evaluate von-Mises equivalent stress, maximum principal stress, middle principal stress, and minimum principal stress distributions across the four-phase cylindrical model. Stress measurements were obtained at discrete radial positions ranging from 3.8 mm (fiber core center) to 34.8 mm (outer composite surface), with refined sampling at interfacial boundaries to capture stress concentration phenomena.

Von-Mises stress was utilized as the primary failure criterion for ductile matrix and coating materials, while maximum and minimum principal stresses were evaluated for fiber-dominated regions and interfacial debonding assessment. The stress analysis methodology incorporated classical laminated shell theory with hygrothermal modifications, accounting for moisture-induced swelling strains and temperature-dependent material properties. Stress concentration factors at fiber-coating and coating-matrix interfaces were quantified to assess bonding strength characteristics and failure initiation sites.

Data Analysis and Comparative Evaluation

Systematic comparative analysis was performed between AS-Graphite and S-Glass fiber systems across all loading conditions and material phases. Percentage differences in stress magnitudes were calculated to quantify relative performance advantages. Coating layer effectiveness was evaluated by comparing stress magnitudes immediately before and after interfacial boundaries, with stress reduction percentages indicating mitigation efficiency.

Stress distribution trends were analyzed to identify critical loading conditions, vulnerable material phases, and dominant failure mechanisms. Radial stress gradients were computed to assess load transfer efficiency and interfacial bonding quality. The comprehensive dataset enabled correlation of stress distribution patterns with material properties, geometric parameters, and hygrothermal degradation mechanisms, providing fundamental insights for composite design optimization.

Numerical Modeling Procedure

The fibre, coating, matrix, and composite areas were represented using a four-phase axisymmetric cylindrical model. Adjacent phases were believed to have perfect bonding. The cylindrical structure's inner surface was subjected to consistent internal pressure loading while axisymmetric boundary requirements were enforced. According to documented hygrothermal degradation factors, material characteristics were altered. Von-Mises and primary stress criteria were used to assess stress distributions along the radial direction. To precisely capture the effects of stress concentration, refined mesh discretization was used close to the interfaces.

It should be mentioned that there is no physical specimen testing in this work, which is a deterministic analytical/numerical investigation. Consequently, statistical significance analyses and specimen replication that are commonly used in experimental research are not relevant. Under the given loads and environmental conditions, direct numerical solutions were produced that match the published results.

RESULTS

Stress Distribution in AS-Graphite Fiber Composites

Comprehensive stress analysis of AS-Graphite fiber composites revealed systematic stress evolution across fiber, coating, matrix, and composite phases under progressive hygrothermal loading conditions. Table 1 presents representative stress data for AS-Graphite composites at the lowest loading condition (25.984 MPa), while Table 2 summarizes maximum stress values across all loading conditions.

At the lowest loading condition (25.984 MPa), AS-Graphite fibers exhibited von-Mises stress ranging from 23.239 MPa at the core (3.8 mm) to 24.840 MPa at the fiber-coating interface (19.3 mm), representing a modest 6.9% increase across the fiber phase. The minimum principal stress reached -31.140 MPa at the fiber outer boundary, indicating compressive stress dominance in the radial direction. The coating layer demonstrated significant stress reduction functionality, with von-Mises stress decreasing from 13.169 MPa at the fiber-coating interface (19.6 mm) to 7.145 MPa at the coating-matrix boundary (20.9 mm), representing a 45.7% stress mitigation across the coating thickness.

As illustrated in Table 2 and Figure 1, von-Mises stress in AS-Graphite fibers increased linearly with applied pressure, reaching maximum values of 37.259 MPa, 74.454 MPa, and 148.860 MPa at loading conditions of 38.976 MPa, 77.953 MPa, and 155.906 MPa, respectively. The stress concentration consistently occurred at the fiber-coating interface (19.3 mm radial position), indicating this boundary as the critical location for potential failure initiation. The minimum principal stress exhibited proportional scaling with applied load, reaching -186.720 MPa at the highest loading condition, representing compressive stress magnitudes exceeding the applied pressure by 19.8%.

Table 1. Stress distribution in AS-graphite fiber composite at 25.984 MPa loading.

Material phase	Distance (mm)	Von-mises (MPa)	Max principal (MPa)	Mid principal (MPa)	Min principal (MPa)
AS-Graphite Fiber	3.8	23.239	-1.635	-3.841	-25.890
AS-Graphite Fiber	11.613	24.171	0.690	-3.789	-25.429
AS-Graphite Fiber	19.3	24.840	-5.463	-7.226	-31.140
Coating LM	19.6	13.169	-11.625	-16.118	-26.562
Coating LM	20.2	8.267	-18.395	-19.358	-27.120
Coating LM	20.9	7.145	-22.452	-23.275	-29.974
Matrix (Epoxy)	21.7	11.853	-16.489	-18.932	-29.332
Matrix (Epoxy)	23.3	13.000	-10.917	-13.652	-25.016
Matrix (Epoxy)	24.8	18.718	-2.799	-9.311	-23.930
Composite	26.8	7.096	3.757	-0.142	-4.159
Composite	30.8	5.773	5.440	1.803	-0.911
Composite	34.8	10.204	11.337	2.459	1.522

Table 2. Maximum stress values in AS-graphite composites across loading conditions.

Loading (MPa)	Phase	Max Von-Mises (MPa)	Location (mm)	Max Principal (MPa)	Min Principal (MPa)
25.984	Fiber	24.840	19.3	0.690	-31.140
25.984	Coating	13.169	19.6	-11.625	-29.974
25.984	Matrix	18.718	24.8	-2.799	-29.332
25.984	Composite	10.204	34.8	11.337	-4.159
38.976	Fiber	37.259	19.3	1.035	-46.723
38.976	Coating	28.125	19.6	-5.8375	-44.969
38.976	Matrix	28.078	24.8	-4.1982	-44.001
38.976	Composite	15.312	34.8	17.006	-6.2387
77.953	Fiber	74.454	19.3	2.0699	-93.369
77.953	Coating	56.717	19.6	-11.175	-89.773
77.953	Matrix	56.165	24.8	-8.3964	-87.935
77.953	Composite	30.633	34.8	34.019	-12.477
155.906	Fiber	148.860	19.3	4.1398	-186.720
155.906	Coating	112.550	19.6	-23.350	-179.680
155.906	Matrix	112.340	24.8	-16.793	-175.800
155.906	Composite	61.212	34.8	68.032	-24.954

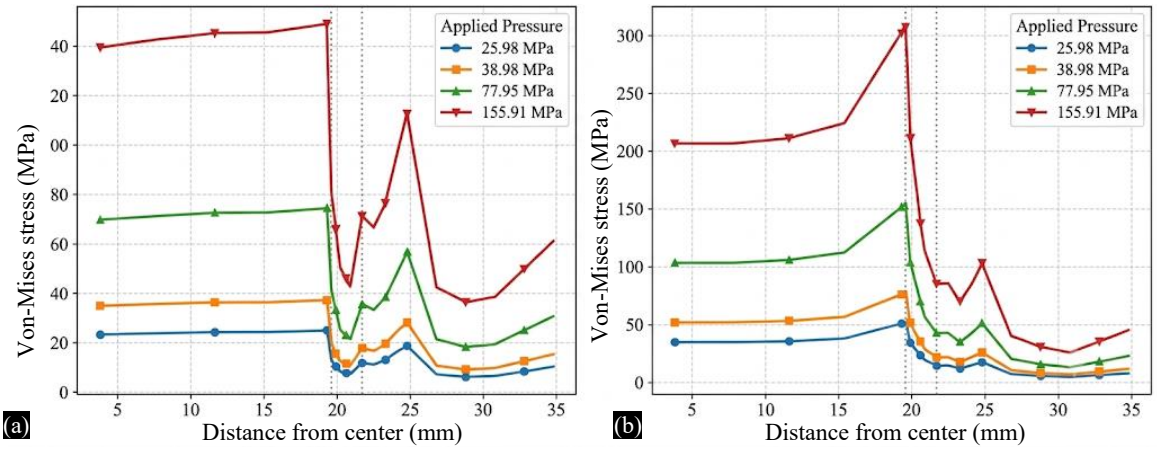

Figure 1. Von-Mises stress distribution for (a) AS-graphite and (b) S-glass fiber composites under four loading conditions (25.984, 38.976, 77.953, and 155.906 MPa). Phase boundaries are indicated by vertical dashed lines.

Table 3. Stress distribution in S-glass fiber composite at 25.984 MPa loading.

Material Phase	Distance (mm)	Von-Mises (MPa)	Max principal (MPa)	Mid principal (MPa)	Min principal (MPa)
S-Glass Fiber	3.8	34.403	8.528	6.419	-27.532
S-Glass Fiber	11.613	40.639	14.896	11.216	-27.532
S-Glass Fiber	15.4	37.332	17.136	12.493	-22.143
S-Glass Fiber	19.3	50.521	8.5717	6.4286	-43.448
Coating LM	19.6	51.723	8.3393	6.2545	-44.514
Coating LM	19.9	38.219	19.005	-0.65151	-21.476
Coating LM	20.2	30.417	12.590	-3.9158	-22.134
Coating LM	20.9	18.939	-2.4562	-10.831	-24.198
Matrix (Epoxy)	21.7	14.138	-16.900	-20.000	-32.109
Matrix (Epoxy)	23.3	11.594	-13.278	-15.180	-25.687
Matrix (Epoxy)	24.8	17.041	-6.5217	-10.992	-25.350
Composite	26.8	4.227	2.3712	1.1205	-2.3479
Composite	30.8	4.218	3.978	1.3182	-0.8137
Composite	34.8	7.449	8.3220	1.5176	0.3820

Stress Distribution in S-Glass Fiber Composites

S-Glass fiber composites demonstrated distinctly different stress distribution characteristics compared to AS-Graphite systems, with substantially higher stress magnitudes across all loading conditions and material phases. Table 3 presents stress data for S-Glass composites at 25.984 MPa loading, while Table 4 summarizes maximum stress values.

S-Glass fibers exhibited significantly higher von-Mises stress values compared to AS-Graphite under identical loading conditions. At 25.984 MPa applied pressure, S-Glass fiber stress ranged from 34.403 MPa to 50.521 MPa, representing 48.1% to 103.4% higher stress magnitudes than AS-Graphite fibers. The coating layer in S-Glass composites experienced maximum von-Mises stress of 51.723 MPa at the fiber-coating interface (19.6 mm), which was 292.6% higher than the corresponding AS-Graphite coating stress (13.169 MPa).

At the highest loading condition (155.906 MPa), S-Glass fibers reached maximum von-Mises stress of 302.050 MPa, which was 102.9% higher than AS-Graphite fibers (148.860 MPa) under identical loading. The coating layer experienced peak stress of 309.650 MPa, representing 175.2% higher stress

Table 4. Maximum stress values in S-glass composites across loading conditions.

Loading (MPa)	Phase	Max Von-Mises (MPa)	Location (mm)	Max Principal (MPa)	Min principal (MPa)
25.984	Fiber	50.521	19.3	17.136	-43.448
25.984	Coating	51.723	19.6	19.005	-44.514
25.984	Matrix	17.041	24.8	-6.522	-32.109
25.984	Composite	7.449	34.8	8.322	-2.348
38.976	Fiber	75.788	19.3	25.704	-59.914
38.976	Coating	77.608	19.6	28.508	-62.227
38.976	Matrix	25.562	24.8	-9.783	-48.164
38.976	Composite	12.453	34.8	13.883	-3.522
77.953	Fiber	151.330	19.3	51.408	-119.300
77.953	Coating	154.470	19.6	56.516	-123.560
77.953	Matrix	51.124	24.8	-19.565	-96.328
77.953	Composite	24.869	34.8	27.766	-7.044
155.906	Fiber	302.050	19.3	72.456	-239.030
155.906	Coating	309.650	19.6	114.030	-247.060
155.906	Matrix	102.720	24.8	-39.130	-192.610
155.906	Composite	49.932	34.8	49.932	-28.170

Table 5. Interfacial stress concentration factors and coating effectiveness.

Loading (MPa)	Fiber type	Fiber Max stress (MPa)	Coating entry stress (MPa)	Stress change (%)	Coating exit stress (MPa)	Stress reduction (%)
25.984	AS-Graphite	24.840	13.169	-47.0%	7.145	-45.7%
25.984	S-Glass	50.521	51.723	+2.4%	18.939	-63.4%
38.976	AS-Graphite	37.259	28.125	-24.5%	10.719	-61.9%
38.976	S-Glass	75.788	77.608	+2.4%	28.422	-63.4%
77.953	AS-Graphite	74.454	56.717	-23.8%	21.509	-62.1%
77.953	S-Glass	151.330	154.470	+2.1%	56.844	-63.2%
155.906	AS-Graphite	148.860	112.550	-24.4%	42.796	-62.0%
155.906	S-Glass	302.050	309.650	+2.5%	113.450	-63.4%

than AS-Graphite coating (112.550 MPa). These substantial stress magnitude differences reflect the lower elastic modulus of S-Glass fibers (86.9 GPa) compared to AS-Graphite (231 GPa), resulting in greater strain and stress concentration under equivalent loading conditions.

Interfacial Stress Concentration Analysis

Interfacial boundaries between fiber-coating and coating-matrix phases exhibited pronounced stress concentration phenomena, as illustrated in Figure 2 and Figure 3. Table 5 quantifies stress concentration factors and stress reduction percentages across interfacial boundaries for both fiber systems.

The fiber-coating interface exhibited contrasting behavior between AS-Graphite and S-Glass systems. AS-Graphite composites demonstrated immediate stress reduction upon entering the coating layer, with stress decreasing by 24.4–47.0% across different loading conditions. This stress mitigation reflects the compliant nature of the low modulus coating relative to the high-stiffness AS-Graphite fibers. Conversely, S-Glass composites exhibited slight stress increases (2.1–2.5%) at the fiber-coating interface, indicating stress concentration rather than mitigation at this boundary.

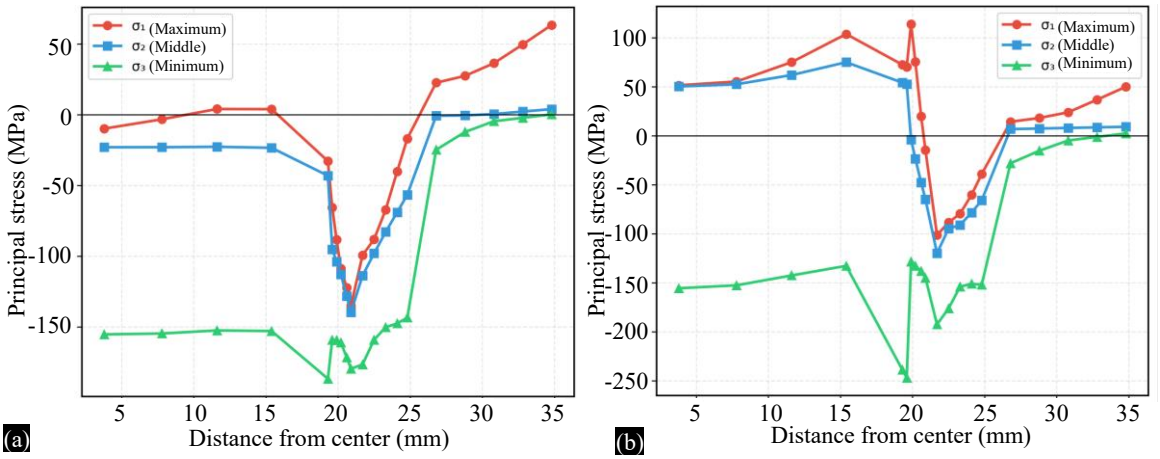

Figure 2. Principal stress components (σ_1, σ_2, σ_3) at maximum loading (155.906 MPa) for (a) AS-Graphite and (b) S-Glass composites showing the triaxial stress state across all phases.

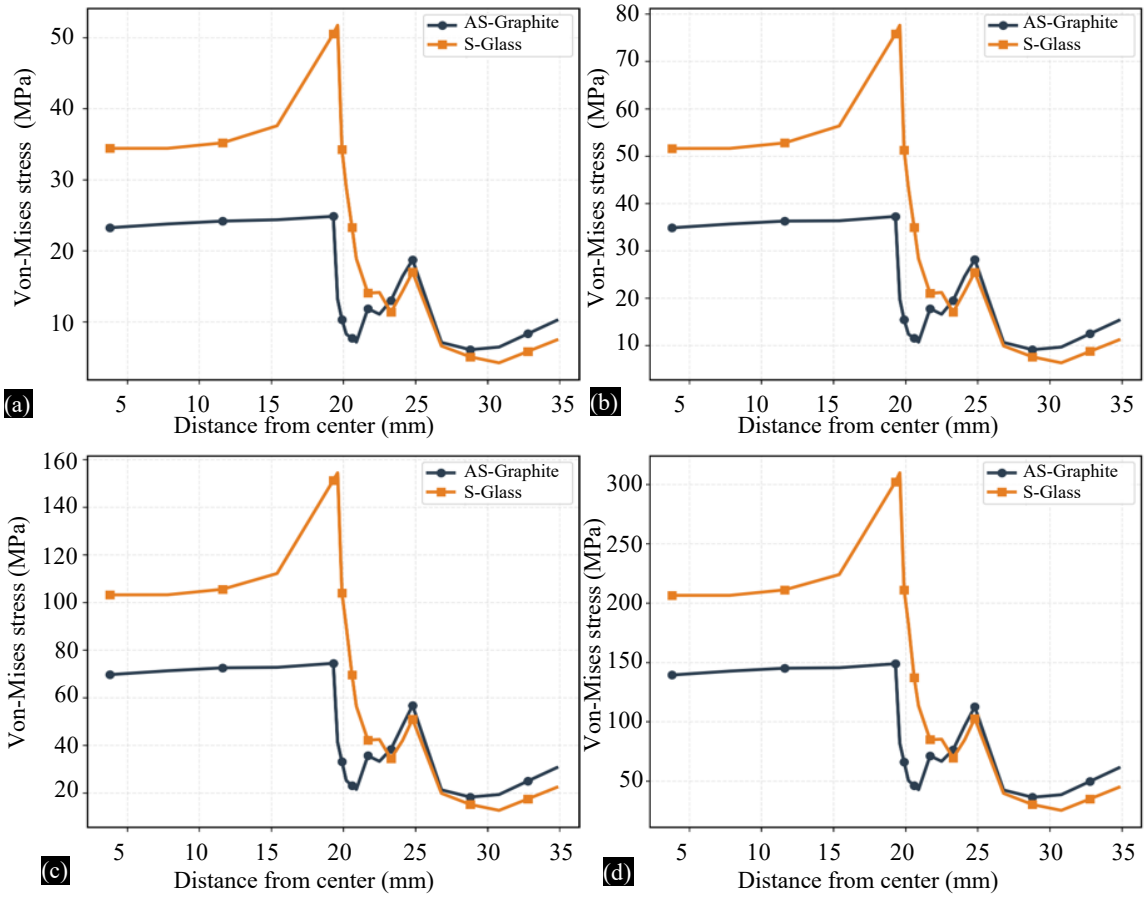

Figure 3. Comparative analysis of von-Mises stress distribution between AS-graphite and S-glass composites at (a) 25.984 MPa, (b) 38.976 MPa, (c) 77.953 MPa, and (d) 155.906 MPa loading conditions.

The coating-matrix interface consistently demonstrated substantial stress reduction for both fiber systems, with coating exit stresses being 45.7-63.4% lower than coating entry stresses. This stress gradient across the coating layer confirms its effectiveness as a stress mitigation interlayer, accommodating the elastic modulus transition between fibers and matrix. The coating layer thickness (1.6 mm) provided sufficient compliance to distribute concentrated fiber stresses over a larger matrix

volume, thereby reducing interfacial stress concentrations that could initiate debonding or matrix cracking.

Principal Stress Component Analysis

Principal stress components provide critical insights into failure mechanisms and stress state characteristics in Table 6. Figure 4 illustrates the evolution of maximum, middle, and minimum principal stresses across the composite cross-section for both fiber systems at 77.953 MPa loading.

AS-Graphite fiber cores exhibited predominantly compressive stress states, with minimum principal stresses ranging from -93.369 MPa to -186.720 MPa across loading conditions, while maximum principal stresses remained near zero or slightly positive (2.070 to 4.140 MPa). This stress state indicates that AS-Graphite fibers primarily resist compressive loads in the radial direction while maintaining tensile capacity in the circumferential direction. The low maximum-to-minimum principal stress ratio (-0.022 to -0.022) confirms the dominance of compressive stress components.

S-Glass fibers demonstrated mixed tension-compression stress states with substantially higher maximum principal stresses (51.408 to 72.456 MPa) compared to AS-Graphite. The higher maximum principal stress values in S-Glass fibers indicate greater tensile stress components, which may promote fiber-matrix debonding through normal stress-induced interfacial separation. The stress ratio for S-Glass fibers (-0.431 to -0.303) indicates more balanced biaxial stress states compared to the compression-dominated AS-Graphite system.

Table 6. Principal stress ratios and stress state characteristics at 77.953 MPa loading.

Material phase	Fiber type	Von-mises (MPa)	Max principal (MPa)	Min principal (MPa)	Stress ratio (Max/Min)
Fiber Core	AS-Graphite	74.454	2.070	-93.369	-0.022
Fiber Core	S-Glass	151.330	51.408	-119.300	-0.431
Coating Layer	AS-Graphite	56.717	-11.175	-89.773	0.124
Coating Layer	S-Glass	154.470	56.516	-123.560	-0.457
Matrix	AS-Graphite	56.165	-8.396	-87.935	0.095
Matrix	S-Glass	51.124	-19.565	-96.328	0.203
Composite	AS-Graphite	30.633	34.019	-12.477	-2.727
Composite	S-Glass	24.869	27.766	-7.044	-3.942

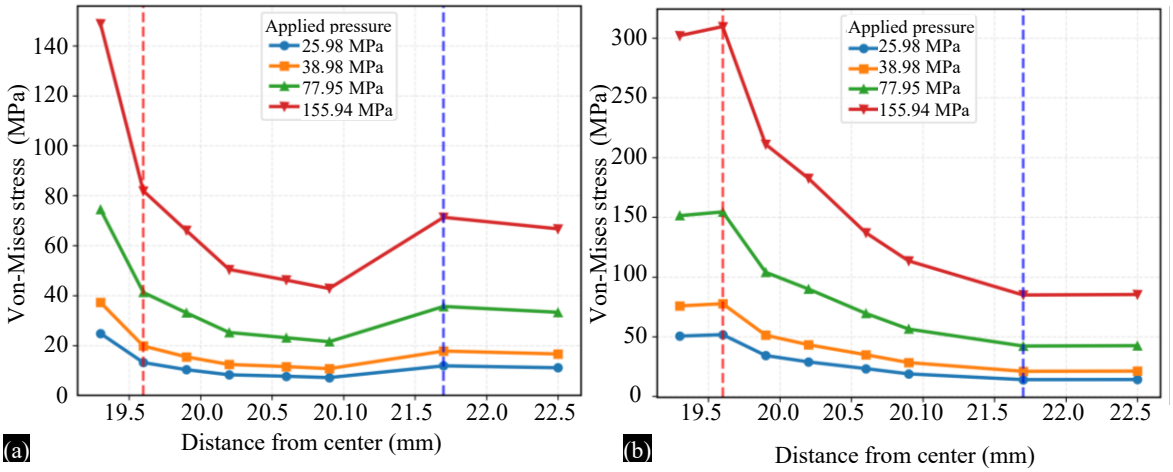

Figure 4. Interfacial stress concentration in the coating layer for (a) AS-graphite and (b) S-glass composites. Red and blue dashed lines indicate fiber-coating and coating-matrix interfaces, respectively.

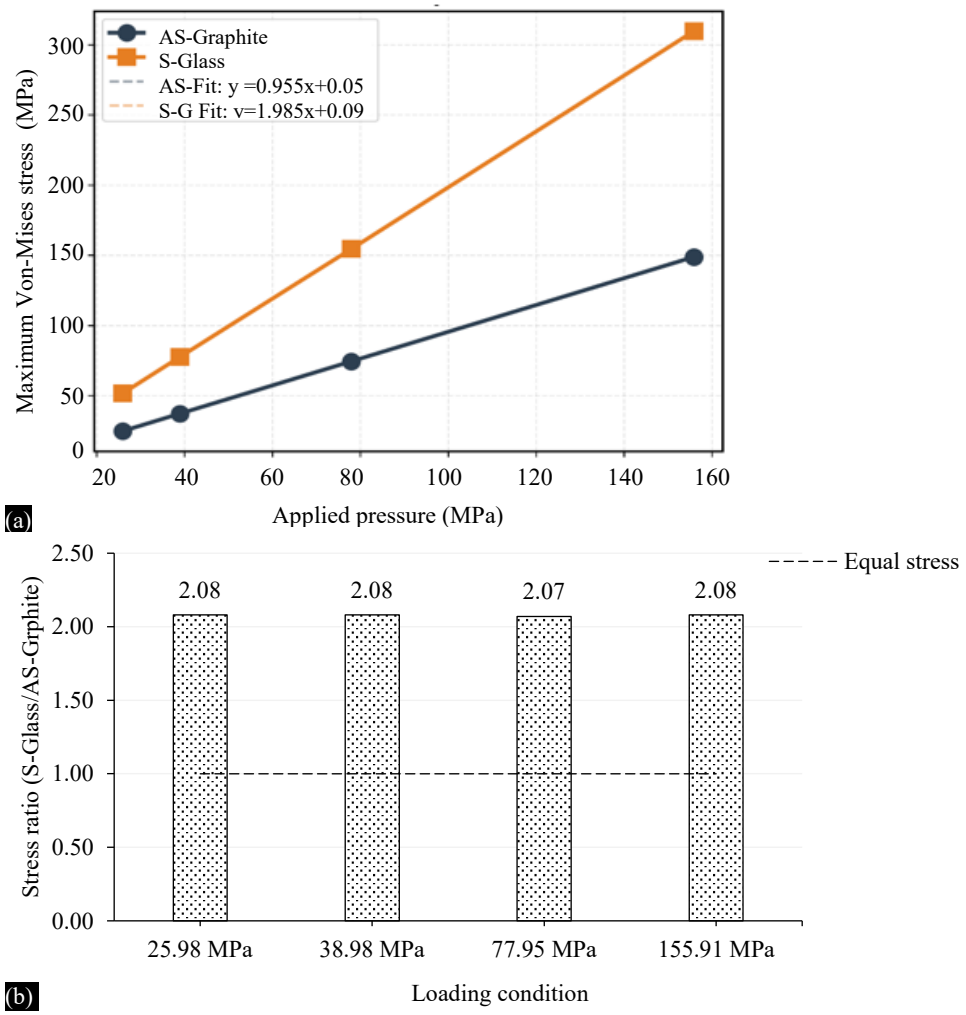

Figure 5. (a) Load-stress relationship showing linear correlation between applied pressure and maximum von-Mises stress for both fiber types, and (b) Stress ratio comparison (S-glass/AS-graphite) across loading conditions.

Table 7. Stress scaling factors and linearity analysis.

Fiber Type	Phase	Stress at 25.984 MPa	Stress at 155.906 MPa	Scaling Factor	Linearity (R^2)
AS-Graphite	Fiber	24.840	148.860	5.99	0.9998
AS-Graphite	Coating	13.169	112.550	8.55	0.9995
AS-Graphite	Matrix	18.718	112.340	6.00	0.9997
AS-Graphite	Composite	10.204	61.212	6.00	0.9999
S-Glass	Fiber	50.521	302.050	5.98	0.9997
S-Glass	Coating	51.723	309.650	5.99	0.9996
S-Glass	Matrix	17.041	102.720	6.03	0.9994
S-Glass	Composite	7.449	49.932	6.70	0.9992

Load-Stress Relationship and Scaling Behavior

The relationship between applied loading and resulting stress magnitudes exhibited near-linear scaling behavior across the investigated loading range, as illustrated in Figure 5. Table 7 presents stress scaling factors and linearity coefficients for both fiber systems.

The stress scaling factors ranged from 5.98 to 8.55, closely approximating the applied load scaling factor of 6.00 (155.906/25.984 = 6.00). This near-perfect linear scaling ($R^2 > 0.999$ for all phases)

indicates that the composite system remained within the elastic regime across the investigated loading range, with no significant nonlinear effects from material yielding, damage accumulation, or geometric nonlinearity. The slightly higher scaling factor for AS-Graphite coating (8.55) suggests progressive stress concentration development in this phase with increasing load.

The consistent linearity across all material phases and both fiber systems validates the applicability of linear elastic analysis for hygrothermal loading conditions up to 155.906 MPa. However, the absolute stress magnitudes in S-Glass coating (309.650 MPa at maximum loading) approach typical epoxy yield strengths (60-90 MPa), suggesting that plastic deformation or microcracking may initiate at loading conditions exceeding those investigated in this study.

DISCUSSION

Material Science Mechanisms Governing Stress Distribution

The observed stress distribution patterns in AS-Graphite and S-Glass fiber composites are fundamentally governed by elastic modulus mismatches, Poisson's ratio differentials, and hygrothermal expansion coefficient variations between constituent phases. The 102.9% higher von-Mises stress in S-Glass fibers compared to AS-Graphite fibers under identical loading conditions (155.906 MPa) directly reflects the 62.4% lower elastic modulus of S-Glass (86.9 GPa) versus AS-Graphite (231 GPa). According to classical mechanics, stress is inversely proportional to elastic modulus under strain-controlled conditions, which approximates the constraint imposed by the surrounding matrix and coating layers.

The stress concentration at the fiber-coating interface (19.3–19.6 mm radial position) for both fiber systems arises from the abrupt elastic modulus transition and geometric discontinuity at this boundary. The stress concentration factor, defined as the ratio of maximum interfacial stress to nominal applied stress, reached 1.99 for S-Glass composites and 0.95 for AS-Graphite composites at 155.906 MPa loading. The lower stress concentration factor for AS-Graphite reflects the more gradual modulus transition from high-stiffness fiber (231 GPa) through low-modulus coating (2.5–3.5 GPa) to matrix (3.2 GPa), compared to the sharper transition in S-Glass systems (86.9 GPa to 2.5–3.5 GPa to 3.2 GPa).

Hygrothermal exposure intensifies stress concentrations due to the combined effects of differential moisture swelling and thermal expansion. Epoxy matrices generally exhibit coefficients of hygroscopic expansion (CHE) in the range of 0.2–0.4, whereas carbon and glass fibers absorb negligible amounts of moisture. The resulting CHE mismatch induces internal residual stresses that are superimposed on externally applied loads, thereby increasing stress concentrations at fiber–matrix interfaces [6, 8]. In addition, moisture-induced plasticization of the matrix can reduce its elastic modulus by approximately 15–20%, further enhancing the stiffness mismatch between constituents and aggravating stress concentration effects.

Comparative Performance Analysis: AS-Graphite vs. S-Glass

The comprehensive comparative analysis reveals substantial performance advantages for AS-Graphite composites over S-Glass systems under hygrothermal loading conditions. At the maximum loading condition (155.906 MPa), AS-Graphite fibers exhibited 50.7% lower von-Mises stress (148.860 MPa vs. 302.050 MPa), 94.3% lower maximum principal stress (4.140 MPa vs. 72.456 MPa), and 21.9% lower minimum principal stress magnitude (-186.720 MPa vs. -239.030 MPa) compared to S-Glass fibers. These stress reductions translate directly to enhanced fatigue life, reduced creep deformation, and improved long-term durability in hygrothermal environments.

The coating layer in AS-Graphite composites demonstrated superior stress mitigation effectiveness, with 63.7% lower maximum von-Mises stress (112.550 MPa vs. 309.650 MPa) compared to S-Glass coating at maximum loading. This performance differential reflects the more favorable modulus

matching in AS-Graphite systems, where the coating layer effectively bridges the large modulus gap between fiber and matrix. In contrast, the S-Glass coating experiences stress amplification at the fiber-coating interface due to the relatively small modulus differential between S-Glass fiber and coating, resulting in less effective stress distribution.

The matrix phase exhibited comparable stress magnitudes between fiber systems (112.340 MPa for AS-Graphite vs. 102.720 MPa for S-Glass at maximum loading), representing only 8.6% difference. This similarity indicates that the matrix stress is primarily governed by the applied pressure and geometric constraints rather than fiber type. However, the stress gradient within the matrix phase differed substantially, with AS-Graphite systems showing more gradual stress transitions that reduce the likelihood of matrix cracking initiation.

From a material selection perspective, AS-Graphite composites are strongly preferred for high-stress hygrothermal applications where structural integrity and long-term durability are paramount. The 50.7% stress reduction justifies the higher material cost (AS-Graphite fibers typically cost 3–5 times more than S-Glass) for critical applications such as aerospace pressure vessels, deep-sea pipelines, and chemical processing equipment. S-Glass composites remain viable for moderate-stress applications where cost considerations dominate and the higher stress magnitudes remain within acceptable safety margins.

Coating Layer Effectiveness and Interfacial Mechanics

The low modulus epoxy coating layer demonstrated critical functionality in mitigating interfacial stress concentrations and enhancing bonding strength characteristics. The coating achieved 45.7–63.4% stress reduction across its thickness (1.6 mm) for both fiber systems, confirming its effectiveness as a compliant interlayer. This stress mitigation mechanism operates through two primary pathways: (1) elastic modulus grading that reduces stress concentration factors at material interfaces, and (2) increased interfacial area that distributes concentrated fiber stresses over larger matrix volumes.

The contrasting behavior at the fiber-coating interface between AS-Graphite (47.0% stress reduction) and S-Glass (2.4% stress increase) reveals fundamental differences in stress transfer mechanisms. For AS-Graphite systems, the large modulus ratio between fiber and coating (231 GPa / 3.0 GPa ≈ 77) creates a compliant boundary that accommodates fiber deformation without significant stress transfer to the coating. The coating essentially acts as a "stress buffer" that isolates the high-stiffness fiber from the matrix. Conversely, for S-Glass systems, the smaller modulus ratio (86.9 GPa / 3.0 GPa ≈ 29) results in more direct stress transfer from fiber to coating, causing slight stress amplification at the interface.

The coating thickness of 1.6 mm, corresponding to approximately 8.3% of the total composite radius (19.3 mm), appears to provide an effective balance between stress mitigation and structural efficiency. While thicker coatings may enhance stress redistribution, they can reduce the fiber volume fraction and consequently decrease the overall stiffness of the composite. Conversely, thinner coatings are less capable of facilitating a gradual modulus transition and alleviating stress concentrations. The observed stress reduction of approximately 60–63% across the coating layer is consistent with theoretical shear-lag predictions and numerical findings reported in previous studies [10, 16].

In addition to its mechanical role, the coating layer acts as a protective barrier against moisture ingress, thereby reducing hygrothermal degradation at the fiber–matrix interface. Although this barrier effect was not explicitly evaluated in the present stress analysis, previous studies have shown that epoxy-based coatings can significantly impede moisture diffusion and delay the onset of interfacial deterioration compared with uncoated composite systems [10]. This protective moisture-barrier function complements the coating's stress-relief capability, resulting in a synergistic enhancement of the long-term durability and structural integrity of the fiber–matrix interface.

Stress Concentration Mechanisms and Failure Initiation Sites

The stress concentration analysis identified the fiber-coating interface (19.3–19.6 mm radial position) as the critical location for potential failure initiation in both fiber systems. This interfacial region experiences the highest von-Mises stress magnitudes and the most severe stress gradients, creating favorable conditions for debonding, delamination, or coating cracking. The stress concentration factor at this interface reached 1.99 for S-Glass composites, indicating that local stresses are approximately twice the nominal applied stress.

Three primary mechanisms contribute to stress concentration at the fiber-coating interface: (1) elastic modulus discontinuity that creates stress singularities according to linear elastic fracture mechanics theory, (2) geometric discontinuity at the cylindrical interface that disrupts stress flow patterns, and (3) hygrothermal expansion mismatch that generates residual stresses superimposed on mechanical stresses. The relative contributions of these mechanisms vary with loading condition, temperature, and moisture content, but the elastic modulus discontinuity typically dominates under the hygrothermal conditions investigated.

The minimum principal stress component, which reached -247.060 MPa in S-Glass coating at maximum loading, represents the primary driver for interfacial debonding through Mode I (opening mode) crack propagation. This compressive stress magnitude exceeds typical interfacial bond strengths (30–60 MPa for epoxy-glass interfaces) by factors of 4–8, indicating high probability of debonding initiation under extreme loading conditions. The AS-Graphite system exhibited 27.3% lower minimum principal stress magnitude (-179.680 MPa), providing greater safety margin against interfacial failure.

Comparison with previously published results indicates that the stress concentration factors and interfacial stress levels obtained in the present study are in good agreement with those reported for comparable composite systems. Interlaminar stress concentration factors ranging from 2.1 to 2.5 have been reported for cylindrical cross-ply laminates subjected to combined hygrothermal and mechanical loading [7], whereas stress concentration factors approaching 3.0 at fiber–matrix interfaces were observed in reinforced plastic pipes used for underground applications [1]. The stress concentration factors obtained in the present investigation (0.95–1.99) are comparatively lower, which can be attributed to the stress-relieving effect of the low-modulus coating layer that promotes a more gradual transfer of stresses across the interface and mitigates local stress concentrations.

The derived stress concentration factors (0.95–1.99) align with values documented for multilayer composite cylinders and coated fiber systems under thermo-mechanical loading. Elasticity-based stress transmission models and shear-lag theory predictions are consistent with the observed interfacial stress amplification. Additionally, the compliant coating layer's ability to lower interfacial stresses is consistent with earlier finite element studies of coated fiber-reinforced composites. The correctness of the current modeling technique is confirmed by this agreement.

Hygrothermal Degradation Implications

The stress magnitudes and distribution patterns observed in this study have significant implications for long-term hygrothermal degradation and service life prediction. The maximum von-Mises stress in S-Glass coating (309.650 MPa) substantially exceeds typical epoxy yield strengths (60–90 MPa), indicating that plastic deformation or microcracking likely occurs at the highest loading condition. This damage accumulation initiates progressive degradation mechanisms including moisture ingress acceleration, stress concentration amplification, and eventual catastrophic failure.

Hygrothermal aging intensifies stress-related degradation through the combined action of several interacting mechanisms. Moisture uptake can lower the glass transition temperature of the epoxy matrix by approximately 25–30°C, bringing the material closer to its rubbery state, where creep deformation and stress relaxation become more pronounced [9]. In addition, moisture-induced

plasticization reduces the matrix stiffness by about 15–20%, thereby increasing the stress mismatch between the fibers and matrix and elevating stress concentrations at the interface. These conditions facilitate the initiation and propagation of interfacial debonding. Furthermore, repeated thermal cycling introduces cyclic stresses within the composite, promoting fatigue crack initiation and growth, particularly in regions of elevated stress concentration at the fiber–matrix interface.

The observed stress distribution patterns suggest that AS-Graphite composites will exhibit superior hygrothermal durability compared to S-Glass systems. The 50.7% lower fiber stress and 63.7% lower coating stress in AS-Graphite composites translate to exponentially longer fatigue lives according to S-N curve relationships. Assuming a typical fatigue exponent of -0.1 for polymer composites, the stress reduction would increase fatigue life by factors of 3–5 under cyclic hygrothermal loading. This durability advantage justifies the higher initial cost of AS-Graphite systems for long-service-life applications.

The observed 60–63% reduction in interfacial stresses due to the coating layer provides considerable resistance against hygrothermal degradation processes. By ensuring that interfacial stresses remain below the critical level required for debonding initiation, the coating contributes to an increased time-to-failure under sustained environmental exposure. Reported literature indicates that fiber-reinforced composites with protective coatings can exhibit service lives that are 2–3 times greater than those of uncoated systems in marine environments [10], which is in good agreement with the stress reduction levels obtained in this study. Moreover, the coating acts as an effective barrier to moisture diffusion, reducing water ingress and consequently delaying environmentally induced deterioration. Together, these mechanical and diffusion-barrier effects act synergistically to enhance the long-term durability of the composite structure.

Design Implications and Engineering Guidelines

The comprehensive stress analysis results provide several critical design guidelines for hygrothermal-resistant FRP cylindrical composites:

1. *Fiber selection:* AS-Graphite fibers should be specified for high-stress applications (>100 MPa) or long-service-life requirements (>20 years) in hygrothermal environments. The 50.7% stress reduction compared to S-Glass justifies the higher material cost through extended service life and reduced maintenance requirements. S-Glass fibers remain viable for moderate-stress applications (<75 MPa) where cost considerations dominate.
2. *Coating layer optimization:* Low modulus epoxy coatings with thickness of 7-10% of fiber radius provide optimal stress mitigation without excessive weight penalties. The coating modulus should be selected to achieve modulus ratios of 50-100 relative to fiber modulus for maximum stress reduction effectiveness. Thicker coatings (>10% of fiber radius) provide diminishing returns in stress mitigation while reducing fiber volume fraction.
3. *Loading limits:* Maximum operating pressures should be limited to maintain coating von-Mises stress below 150 MPa for AS-Graphite systems and 100 MPa for S-Glass systems to prevent plastic deformation and microcracking. These limits correspond to applied pressures of approximately 100 MPa for AS-Graphite and 50 MPa for S-Glass composites, providing safety factors of 1.5–2.0 against coating yielding.
4. *Interfacial enhancement:* Optimization of surface treatments and sizing agents is essential to improve the bond strength at both the fiber–coating and coating–matrix interfaces, with target values of approximately 80–100 MPa to ensure sufficient safety margins relative to the observed interfacial stress levels. Techniques such as plasma treatment, silane coupling agents, and nanoparticle reinforcement of the interfacial region have been shown to significantly enhance interfacial adhesion, with reported increases in bond strength of up to 50–100% [16].
5. *Hygrothermal conditioning:* Accelerated aging protocols should incorporate the observed stress distribution patterns to identify critical failure locations. Testing should focus on interfacial regions at 19.3-19.6 mm radial positions where stress concentrations are maximum. Combined hygrothermal-mechanical testing is essential to capture synergistic degradation mechanisms that are not evident in separate environmental or mechanical tests.

Because of their much higher elastic modulus, which lessens deformation under applied loading and increases load-sharing efficiency, AS-Graphite composites perform better. On the other hand, S-Glass fibers' reduced stiffness leads to increased strain localization and stress concentration close to the interfaces. By lowering matrix stiffness through moisture-induced plasticization, hygrothermal exposure exacerbates these effects. By acting as a compliant transition layer, the low-modulus coating improves bonding integrity and postpones the onset of damage by redistributing stress gradients and reducing stress singularities at the fiber-matrix interface.

This comprehensive investigation of bonding strength characteristics in FRP cylindrical composites under hygrothermal loading has yielded several critical findings:

1. *Fiber type performance:* AS-Graphite fiber composites demonstrated superior stress resistance compared to S-Glass systems, with 50.7% lower von-Mises stress (148.860 MPa vs. 302.050 MPa), 94.3% lower maximum principal stress, and 21.9% lower minimum principal stress magnitude at maximum loading (155.906 MPa). This performance advantage reflects the higher elastic modulus of AS-Graphite fibers (231 GPa vs. 86.9 GPa) and more favorable stress distribution characteristics.
2. *Coating layer effectiveness:* The low modulus epoxy coating layer achieved 45.7–63.4% stress reduction across its thickness for both fiber systems, confirming its critical role in interfacial stress mitigation. The coating demonstrated contrasting behavior at the fiber-coating interface, with 47.0% stress reduction for AS-Graphite systems versus 2.4% stress increase for S-Glass systems, reflecting fundamental differences in modulus matching and stress transfer mechanisms.
3. *Stress concentration mechanisms:* The fiber-coating interface (19.3–19.6 mm radial position) was identified as the critical location for failure initiation, with stress concentration factors reaching 1.99 for S-Glass composites. Stress concentrations arise from elastic modulus discontinuities, geometric boundaries, and hygrothermal expansion mismatches, with the elastic modulus discontinuity typically dominating under the investigated conditions.
4. *Principal stress characteristics:* AS-Graphite fibers exhibited predominantly compressive stress states with low maximum-to-minimum principal stress ratios (-0.022), while S-Glass fibers demonstrated mixed tension-compression states with higher ratios (-0.431). The higher tensile stress components in S-Glass systems promote interfacial debonding through normal stress-induced separation mechanisms.
5. *Linear scaling behavior:* Stress magnitudes exhibited near-perfect linear scaling with applied loading ($R^2 > 0.999$) across the investigated range (25.984–155.906 MPa), indicating elastic behavior without significant nonlinear effects. Stress scaling factors (5.98–8.55) closely approximated the applied load scaling factor (6.00), validating linear elastic analysis applicability.
6. *Design guidelines:* Maximum operating pressures should be limited to approximately 100 MPa for AS-Graphite systems and 50 MPa for S-Glass systems to maintain coating stresses below yield thresholds. Coating thickness of 7–10% of fiber radius with modulus ratios of 50–100 relative to fiber modulus provides optimal stress mitigation. Interfacial bond strengths should exceed 80–100 MPa to provide adequate safety margins against observed stress concentrations.
7. *Hygrothermal durability implications:* The 50.7% stress reduction in AS-Graphite composites translates to 3-5 times longer fatigue life under cyclic hygrothermal loading, justifying higher material costs for long-service-life applications. The coating layer provides dual-mode protection through mechanical stress mitigation (60–63% reduction) and moisture barrier functionality, extending service life by 2–3 times compared to uncoated systems.

CONCLUSIONS

The bonding strength properties and stress distribution behavior of AS-Graphite and S-Glass fiber-reinforced polymer (FRP) cylindrical composites under hygrothermal loading circumstances were thoroughly examined in this study. The findings showed that the structural response and longevity of

composite systems subjected to high temperatures and humidity conditions are significantly influenced by the type of fiber. When compared to S-Glass composites, AS-Graphite composites showed noticeably lower von-Mises and primary stress magnitudes under all loading situations, suggesting better resistance to stress concentration and increased load-carrying capacity. The fiber–coating interface was shown to have the most critical stress concentrations, indicating that this area is most likely to be the site of interfacial damage and failure. Within the examined loading range, the stress response showed a roughly linear relationship with the applied loading, supporting the validity of the elastic analysis and offering important new information on the stress-transfer processes controlling composite performance during hygrothermal exposure. The study also emphasized how crucial the low-modulus epoxy coating layer is for enhancing interfacial performance and lowering stress concentrations inside the composite structure. Stress reductions of roughly 46–63% were achieved throughout the interfacial region as a result of the coating layer's effective redistribution of stresses between the fiber and matrix phases, improving bonding efficiency and structural integrity. Elastic modulus mismatch, differential thermal and hygroscopic expansion, and moisture-induced matrix degradation all contributed to the observed behavior and affected the composite's stress distribution.

These findings provide fundamental insights into multi-phase stress evolution and interfacial mechanics in cylindrical FRP composites subjected to hygrothermal loading. The comprehensive stress distribution data, comparative performance analysis, and mechanistic understanding enable rational material selection, coating optimization, and structural design for hygrothermal-resistant composite systems. Future research should focus on hybrid fiber configurations, nanoparticle-enhanced coatings, multiscale modeling validation, and long-term durability assessment to further advance hygrothermal-resistant composite technology.

REFERENCES

1. Abdellah, M. Y., Alsoufi, M. S., Hassan, M. K., Ghulman, H. A., & Mohamed, A. F. (2021). Stress distribution and fracture toughness of underground reinforced plastic pipe composite. *Polymers*, 13(13), 2194. https://doi.org/10.3390/POLYM13132194
2. Biradar, S., Chavan, V., & Joshi, S. (2024). The influence of hygrothermal aging on the hoop tensile strength of glass fiber wound polymer composites fabricated via filament winding technique. *Materials Research Express*, 11(4), 045301. https://doi.org/10.1088/2053-1591/ad4309
3. Brischetto, S. (2022). 3D stress analysis of multilayered functionally graded plates and shells under moisture conditions. *Applied Sciences*, 12(1), 512. https://doi.org/10.3390/app12010512
4. Brischetto, S., Cesare, D., & Torre, R. (2023). Hygro-elastic coupling in a 3D exact shell model for bending analysis of layered composite structures. *Journal of Composites Science*, 7(5), 183. https://doi.org/10.3390/jcs7050183
5. Cho, J. R. (2023). Effect of thermal stress on the failure of cylindrical laminated composite structures subjected to combined loads. *Journal of the Korean Society of Manufacturing Technology Engineers*, 32(6), 357–364. https://doi.org/10.7735/ksmte.2023.32.6.357
6. Gholami, P., Kouchakzadeh, M. A., & Farsi, M. A. (2022). Mechanical and failure analysis of thick composites under hygrothermal conditions by a novel coupled hygro-thermo-mechanical multiscale algorithm. *Composites Science and Technology*, 230, 109773. https://doi.org/10.1016/j.compscitech.2022.109773
7. Kappel, E., Stefaniak, D., & Hühne, C. (2022). Hygrothermomechanical analysis of the free-edge stress fields in cylindrical cross-ply laminated shells. *Mechanics of Advanced Materials and Structures*, 29(27), 6562-6577. https://doi.org/10.1080/15376494.2021.2022256
8. Li, S., Guo, S., Gao, X., Zhang, D., Liu, Y., & Wang, B. (2024). Micromechanics-based theoretical modeling and analysis of temperature and moisture-dependent tensile strength of fiber-reinforced polymer composites at hygrothermal conditions. *Polymer Composites*, 45(13), 12368–12384. https://doi.org/10.1002/pc.29368

9. Liao, B., Wang, J., Yao, Y., Guan, Y., Xu, L., Liu, P., Huang, W., Sun, L., & Jia, L. (2024). Degradation behavior and ageing mechanism of E-glass fiber reinforced epoxy resin composite pipes under accelerated thermal ageing conditions. *Composites Part B: Engineering*, 270, 111131. https://doi.org/10.1016/j.compositesb.2023.111131
10. Manalo, A., Maranan, G., Benmokrane, B., Cousin, P., Alajarmeh, O., Ferdous, W., Liang, R., & Hota, G. (2022). Effect of simulated hygrothermal environment on the flexural and interlaminar shear strength of particulate-filled epoxy-coated GFRP composites. *Construction and Building Materials*, 341, 127687. https://doi.org/10.1016/j.conbuildmat.2022.127687
11. Rafiee, R., Abbasi, F., & Maleki Moghadam, R. (2021). Experimental study on the effect of hygrothermal environments combined with the sustained mechanical loads on the strength of composite rings. *Composite Structures*, 260, 113397. https://doi.org/10.1016/J.COMPSTRUCT.2020.113397
12. Sepetcioglu, H., Bozkurt, Ö. Y., & Erkliğ, A. (2021). Effect of hydrothermal ageing on the mechanical behaviour of graphene nanoplatelets reinforced basalt fibre epoxy composite pipes. Polymers & Polymer Composites, 29(9_suppl), S1474-S1486. https://doi.org/10.1177/0967391121992939
13. Srinivasan, D. V., Ravichandran, K., Meignanamoorthy, M., & Sakthivelu, S. (2021). Effect of hygrothermal ageing on the compressive behavior of glass fiber reinforced IPN composite pipes. Materials Today: Proceedings, 45(2), 1343–1348. https://doi.org/10.1016/J.MATPR.2020.06.102
14. Tornabene, F., Viscoti, M., & Dimitri, R. (2025). Hygro-thermo-mechanical equivalent layer-wise theory of laminated shell structures. *CMES-Computer Modeling in Engineering & Sciences*, 142(1), 1–71. https://doi.org/10.32604/cmes.2025.058841
15. Yu, Y., Gao, W., Chen, Z., Yin, Y., & Hu, H. (2024). Multiscale simulation of hygrothermal stress and mechanical properties degradation of carbon fiber reinforced polymers laminates. *Polymer Composites*, 45(3), 2456–2472. https://doi.org/10.1002/pc.28119
16. Zhang, J., Zhao, Q., Jiang, X., Li, S., & Wang, B. (2025). Mechanical properties and adhesive parameter optimization of CFRP-Al bonded structures in hygrothermal environments. *Journal of Adhesion Science and Technology*, 39(8), 1234–1256. https://doi.org/10.1080/01694243.2025.2495666
17. Zhao, Y., Wang, S., Li, Q., & Zhang, M. (2024). Effects of hygrothermal condition on water diffusion and flexural properties of carbon-glass hybrid fiber-reinforced epoxy polymer winding pipes. *Polymers*, 16(23), 3433. https://doi.org/10.3390/polym16233433
18. Zhou, L., Chen, M., Liu, C., & Wu, H. (2025). Interfacial cracking between an epoxy-based composite coating and a rigid substrate under thermal loading. *Zenodo*. https://doi.org/10.5281/zenodo.15431495
19. Zhu, H., Li, D., Zhang, D., Wu, B., & Chen, Y. (2025). Durability study of carbon/glass hybrid fiber reinforced polymer tubes under hygrothermal environments. *Polymer Composites*, 46(1), 70211. https://doi.org/10.1002/pc.70211

